# Suction caissons subjected to monotonic combined loading

B. Penzes
*Technical University of Denmark, Kgs Lyngby, Denmark, balint.penzes@gmail.*

M. R. Jensen
*Technical University of Denmark, Kgs Lyngby, Denmark, mellejensen@hotmail.com*

V. Zania
*Technical University of Denmark, Kgs Lyngby, Denmark, vaza@byg.dtu.dk*

ABSTRACT
*Suction caissons are being increasingly used as offshore foundation solutions in shallow and intermediate water depths. The convenient installation method through the application of suction has rendered this type of foundation as an attractive alternative to the more traditional monopile foundation for offshore wind turbines. The combined loading imposed typically to a suction caisson has led to the estimation of their bearing capacity by means of 3D failure envelopes. This study aims to analyse the behaviour of suction caissons for offshore wind turbines subjected to combined loading. Finite element models of the caisson-soil are developed in order to derive the failure envelopes considering both sand and clay profiles. The numerical modelling is being validated by the failure mechanisms reported in the literature for skirted foundations. The sensitivity of the load response curves on the selection of the constitutive soil model is examined. The failure envelopes of a single suction caisson obtained by the numerical models are in good agreement with the corresponding ones suggested by closed-form expressions.*

**Keywords: suction caisson, failure envelope, numerical modelling, combined loading.**

## 1 INTRODUCTION

In the recent years the energy industry has promoted deeper water installations in seek of increased capacity resources. Thus, floating structures and large wind turbine farms have been increasingly developed and this has favored alternative geotechnical solutions like the suction caisson. The suction caisson foundation system has significant advantage regarding the installation time and cost, and the material requirement compared with the traditional foundation systems, like monopiles. It has been extensively used so far as anchor for mooring systems for buoyant platforms in the offshore oil and gas industry (Andersen et al., 2005). Lately suction caissons have been also suggested as foundation for offshore wind turbines either as monopod or as tripod (Houlsby et al., 2005, Senders 2008). The only known suction bucket foundation which supports an offshore wind turbine is the one installed in 2014 as part of the Borkum Riffgrund Wind Farm. In addition, there have been three successfully installed suction buckets which support met-masts (Horns Rev II, Dogger Bank) and some more intended to support platforms. Furthermore, two prototype projects have been carried out (Wilhelmshaven, Frederikshavn).

The suction caisson is open-ended at the bottom and closed at the top, and installed by applying under-pressure within the caisson after it has penetrated into the seabed by self-weight. The suction caissons are typically made of steel and have a length to diameter ratio (L/D) of 1 to 6. One of the design issues of suction caissons is their capacity when subjected to combined loading. The studies of the bearing capacity of suction caissons in clay for combined V-H loading have concluded in analytical expressions of failure

envelopes, as those proposed by Senders and Kay (2002) and by Supachawarote et al., (2004) after finite element analysis. Extensive experimental investigation of suction caissons in loose and dense sand has resulted in failure envelopes for M-V and H-V load combinations (Byrne, 2000), while recently further experimental results suggest a revised form of the M-V failure for dense sands (Larsen et al., 2013).

The present study aims at analyzing numerically the bearing capacity of suction caissons when subjected to combined V-H loading. Three dimensional (3D) finite element models are developed to study the failure mechanisms of suction caissons in dense sand and in normally consolidated clay. In the case of the sand profile, two different constitutive soil models were examined to analyze the effect on the failure mechanism, while in clay two clay profiles, one with an undrained shear strength profile proportional to depth and one with constant shear strength, were considered. The numerical modelling was validated by the failure mechanisms reported in the literature for skirted foundations. Finally, V-H failure envelopes for the chosen loading conditions were developed for both sand and clay and compared with the ones reported in previous studies.

## 2 METHODOLOGY

### *2.1 Numerical modelling*

In this study 3D finite element models of monopod caissons were developed in Plaxis 3D AE (Brinkgreve et al., 2015). Due to the symmetry of the geometry and the loading direction only half of the problem was modelled to reduce the simulation time. The suction caissons were wished in place with 6m of diameter, the length to diameter ratio L/D was 1.0, and they were considered as rigid. The boundary conditions were defined as constrained DOF perpendicular to each lateral plane and fully constrained at the bottom of the soil layer. In order to achieve sufficient accuracy and convergence an additional zone with the depth and radius of 2D was defined and a finer mesh close to the caisson was established after convergence analysis, as shown in Figure 1.

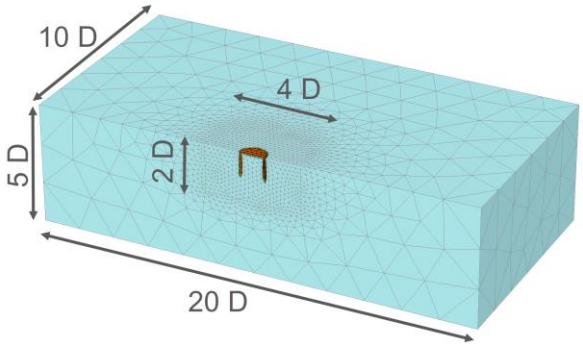


*Figure 1 Finite element model of the suction caisson and boundary conditions*

### *2.2 Soil modelling*

Two soil profiles were considered representative of normally consolidated clay: (a) undrained shear strength increasing proportionally with depth (z), according to $s_u$=4.0+5z kPa and (b) constant undrained shear strength of $s_u$=10.0 kPa. A constant Young modulus ratio was adopted, with $E/s_u$ of 500, and Poisson's ratio was taken as ν = 0.495. The soil parameters for dense sand were the following: the internal angle of friction φ' = 40°, dilation angle ψ = 10° and Poisson's ratio ν = 0.35, cohesion c = 1 kPa. The Young modulus for the Mohr-Coulomb soil model was set to E = 70 MPa. The additional parameters for the HSsmall model (Benz, 2006) are summarized in Table 1. The interface strength properties were assigned to be identical of those of the soil material.

*Table 1 Additional soil properties for dense sand*

| Parameter | Symbol | Value |
|---|---|---|
| Elastic modulus | $E_{50}$ | 28.5 $MPa$ |
| Oedometric modulus | $E_{oed}$ | 35.2 $MPa$ |
| Unloading/Rel. modulus | $E_{ur}$ | 85.6 $MPa$ |
| Initial shear modulus | $G_0$ | 103.5 $MPa$ |
| Ref. shear strain | $\gamma_{0.7}$ | 0.14 $mm/ma$ |
| Earth pressure coefficient | $K_0$ | 0.37 |

### *2.3 Modelling approach*

The analysis included the following calculation steps: (a) the geostatic phase, when initial stresses were established, (b) the installation of the caisson, by activating the

predefined geometry with the positive and negative interfaces in order to simulate the soil-structure interaction, (c) the loading phase, with vertical, horizontal and inclined applied forces, which were concentrated at the center of the caisson with an angle of 30°, 40°, 50°, and 60° from the horizontal axis. In this study the load, or stress controlled approach was applied for the caissons in clay, while for dense sand, the displacement controlled method was used in order to reduce the convergence issues and to minimize the local stress concentrations at the structural edges during the loading.

Special attention has been drawn to the modelling of the frictional material. The plastic potential in this case can be described based on the application of the associated or the non-associated plasticity theories (Chen & Liu, 1990) in the numerical model. In the case of the simple Mohr- Coulomb failure criterion this is translated as the following two cases: (a) the dilation angle is set equal to the friction angle ψ=ϕ' (associated) and (b) the dilation angle is an initially small value or equal to zero ψ=0° (non-associated) (Vaitkunaite et al., 2012 and Lyamin et al., 2007). However, the true behavior of the dense sand is somewhere between (Potts & Zdravkovic 1999 and Vaitkunaite et al., 2012). Hence as suggested by Bolton (1986) and Houlsby (1991) the dilation angle can be given by:

$$\psi = \varphi' - 30° \quad (1)$$

The available solutions in the literature, which are based on two and three dimensional finite element limit analysis considering associated plasticity theory (Lyamin et al., 2007), can be useful as validation to the adopted numerical modelling approach. Therefore in the present study the axial bearing capacity was investigated on the basis of both plasticity theories. A parametric study was performed to examine the effect of the dilation angle (ψ=ϕ'; ψ=0°; ψ= ϕ'-30°) and the strengthening of the interface element in case of both plasticity theories.

The results of this investigation indicated that a good balance between convergence and accuracy could be obtained for the non-associated model (ψ= ϕ'-30°) which was further applied for the combined loading and the effect of the Mohr-Coulomb and the HSsmall models were studied in case of dense sand.

## 3 DISCUSSION AND RESULTS

### *3.1 Axial bearing capacity in dense sand*

At first the axial bearing capacity was investigated considering the associated plasticity theory, which meant that the dilation angle was set as ψ=ϕ'=40°. Several convergence issues emerged in this attempt, and a feasible solution was pursued by: (a) changing different numerical control parameters, (the solver, and the arc-length control types as suggested in Brinkgreve et al., 2015), and (b) examining the sensitivity to the strength of the interface and the soil shear strength properties. Nevertheless, none of the above mentioned variations could reach a numerically acceptable outcome. Thereafter the dilation angle was set to zero (ψ=0°) and following Eq (1) as ψ=10° in order to model the non-associated plasticity theory. In this case, convergence issues were met at an early stage of the loading. These issues were attributed to the shear failure along the interfaces, which did not allow the application of higher loading. As a result, the soil bearing capacity was not fully mobilized and the ultimate load could not be assessed. A parametric study was carried out in order to investigate the effect of a strengthened interface on the failure mechanism. As a result of this parametric analysis the cohesion of 70 kPa in the interface was found adequate without any influence on the bearing capacity.

*Table 2 The axial bearing capacity of the symmetric caisson foundation in sand*

| $V^{ult\ (Lyman\ et\ al.)}_{associated}$ $(\psi = 40°)$ | $V^{max\ (Plaxis\ 3D)}_{non-associated}$ $(\psi = 0°)$ | $V^{ult\ (Plaxis\ 3D)}_{non-associated}$ $(\psi = 10°)$ |
|---|---|---|
| $661 \cdot 10^3\ kN$ | $660 \cdot 10^3\ kN$ | $744 \cdot 10^3\ kN$ |

In Table 2 the ultimate bearing capacity is reported for the various dilation angles considered in this study. The calculated value based on Lyamin et al. (2007) provides an

indication of the load based on the associated plasticity theory. It can be observed that the vertical ultimate load of the non-associated model is significantly larger, which emphasize, that the axial bearing capacity is highly depend on the dilation angle (Houlsby, 1991).

### *3.2 Combined V-H loading in dense sand*

The failure mechanisms for the dense sand profile were analyzed for inclined loads at $30^o$, $40^o$, $50^o$, and $60^o$ with the horizontal axis. In Figure 2 the incremental deviatoric strains contours depict the failure zones developed for horizontal, vertical and two inclined load cases.

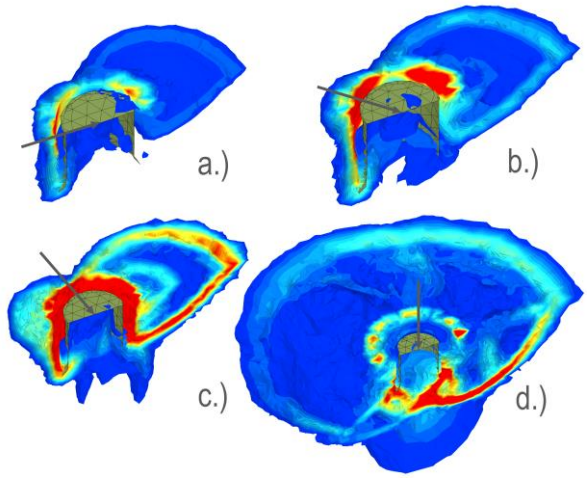


*Figure 2 Failure zones in dense sand (M-C soil model) for (a) horizontal, (b) $30^o$, (c) $60^o$ and (d) vertical load.*

The failure surface does not extend to the tip of the skirt in the horizontal loading case (Figure 2a.) which is probably related to the absence of passive failure. As the inclination of the load increases, the failure wedge extends to the tip of the skirt and further away laterally as well (Figure 2b and 2c). Because of the vertical load component there is some indication of shaft failure around the caisson which is particularly evident in the case of $60^o$ load inclination. A fully developed Prandtl-type failure mechanism was observed in case of vertical loading (Figure 2d), which illustrates a wedge at the caisson tip and an extended failure zone propagating to the soil surface.

The effect of the selected constitutive soil model on the failure surface was also investigated and the corresponding results obtained with the HSsmall soil model are shown in Figure 3.

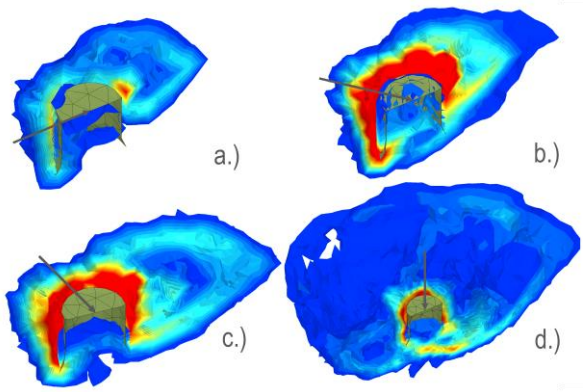


*Figure 3 Failure zones in dense sand (HSsmall soil model) for (a) horizontal, (b) $30^o$, (c) $60^o$ and (d) vertical load.*

The pattern of the deviatoric strain increments is quite similar comparing Figures 2 and 3. However it is clearly visible, that the strain increments are less localized without clearly defined failure surfaces. Furthermore, the failure along the shaft is quite extensive (Figure 3b and 3c). This is also apparent in case of the pure vertical loading (Figure 3d) while the failure surface around the caisson is not clearly defined.

The load-displacement curves derived for the examined load inclinations and the two constitutive models are shown in Figure 4. It can be observed that smaller displacements are required to reach failure in the case of the HSsmall model compared to the Mohr-Coulomb case. The difference becomes more apparent as the loading inclination increases, thus the largest deviation occurred in case of $60^o$ load inclination.

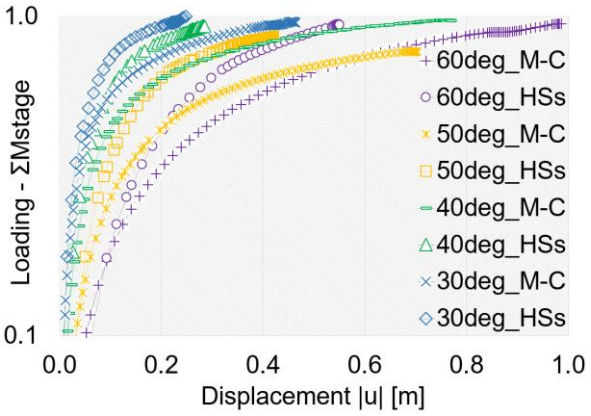


*Figure 4 Load-displacement curves for inclined loading in case of dense sand*

The ultimate load (resultant) was estimated and the results are summarized in Table 3. The difference in the ultimate load, when comparing the two constitutive models, is within the range of 10%. Considering the fact that the yield criterion for both models is identical, the discrepancy is attributed to the extent of the failure surface within the soil mass, especially in the cases of 30°, 40°, and 50° load.

*Table 3 The ultimate bearing capacity in case of M-C and HSsmall soil models*

| ***Inclination*** | $V^{ult}_{M-C}$ ***[kN]*** | $V^{ult}_{HSsmall}$ ***[kN]*** | **Difference** |
|---|---|---|---|
| 90° | $744 \cdot 10^3$ | $748 \cdot 10^3$ | 0.5 % |
| 60° | 52250 | 56400 | 7.4 % |
| 50° | 33600 | 30450 | 9.4 % |
| 40° | 19400 | 18600 | 4.1 % |
| 30° | 13152 | 13150 | 0.01 % |
| 0° | 7546 | 8550 | 11.7% |

In order to ensure a general comparison of the results the non-dimensional failure envelope (Figure 5) of the vertical and horizontal loads (V-H failure envelope) was developed.

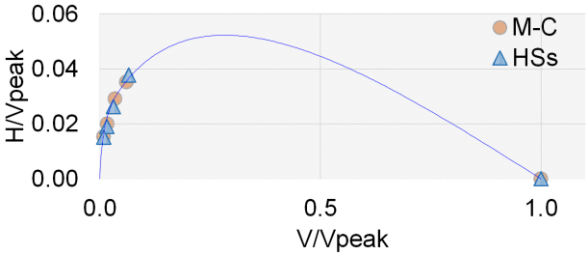


*Figure 5 Yield surface for the caisson under inclined loading*

The combined failure envelope was established by normalizing the ultimate loads by the vertical ultimate load as suggested by Byrne (2000) in case of suction caissons. The numerical results compare well regarding the shape obtained by experimental results (Byrne, 2000). However, it is recommended in the literature to apply data from field-measurements and swipe experimental tests (Butterfield & Gottardi, 2003) in order to find the appropriate yield curves (Byrne, 2000).

### *3.3 Axial, lateral and inclined bearing capacity in clay*

The axial and lateral capacity of the suction caisson has been estimated considering a linearly increasing and a constant undrained strength profile. The results reported in Table 4 indicate a higher capacity for the linearly increasing soil strength profile. The axial bearing capacity for the constant profile indicate that $N_c$=9.1, which is consistent with results of plane strain analyses for skirted foundations presented by Yun & Bransby (2007). However the calculated $N_c$=8.4 for the linear increasing profile is higher than the corresponding value reported in the same study.

*Table 4 Axial and lateral bearing capacity for suction caisson in clay*

| ***Soil profile*** | $H_0$ ***[kN]*** | $V_0$ ***[kN]*** |
|---|---|---|
| ***Linear*** | 1599 | 8101 |
| ***Constant*** | 988 | 2564 |

Inclined loading was applied on the suction caisson for a number of angles with respect to the horizontal axis (10°, 30°, 40°, 50°, 60°, and 80°). The deviatoric strain increment contours indicate the generated failure mechanisms as shown in Figure 6 and Figure 7 for linearly increasing and constant $s_u$ respectively.

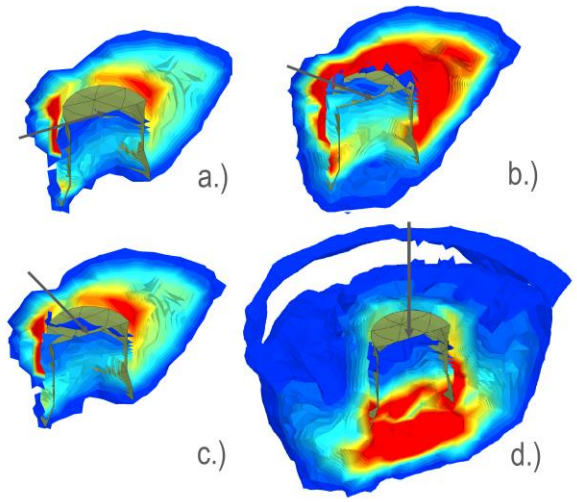


*Figure 6 Failure mechanisms in clay with linear increasing undrained shear strength, for (a) horizontal, (b) 30°, (c) 60° and (d) vertical load.*

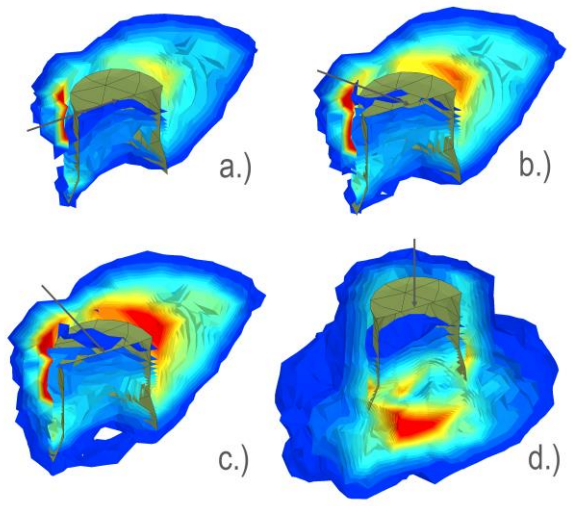


*Figure 7 Failure mechanisms in clay with uniform undrained shear strength for (a) horizontal, (b) 30°, (c) 60° and (d) vertical load.*

It is observed that the increase of the loading angle causes increased strains below the caisson tip. In the lateral load case the strain increase is localized in the passive side. At the 30° loading angle (Figure 6 b.) the failure surface extended further out on the passive side. The progress in the failure mechanism is almost the same for the clay with uniform undrained shear strength. As the load inclination increases from the horizontal axis the failure surface expands on the passive side and when the load reaches pure vertical the failure surface is concentrated beneath the suction caisson. Comparing the failure mechanisms for the two different normally consolidated clay profiles, the main difference appears when the loading has an inclination angle of 30°.

On the load-displacement curves shown in Figure 8 the loading stages are represented in order to observe the required displacements to fully mobilize the soil capacity. It is observed that displacement required to mobilize the ultimate capacity is independent of the shear strength profile. On the other hand as the load inclination increases the ultimate capacity is reached at higher displacements. At every case the ultimate axial and lateral load were defined and the results are summarized in Table 4.

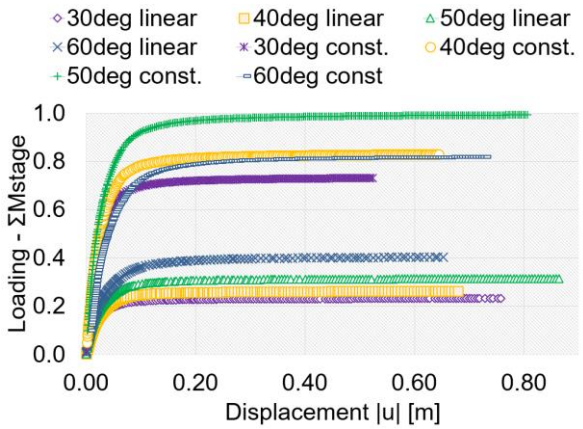


*Figure 8 Load-displacement curves for inclined loading in case of clay*

*Table 4 Bearing capacity for inclined loading of suction caisson in clay with linear increasing shear strength profile*

| ***Inclination*** | $H\ [kN]$ | $V\ [kN]$ | $V_{lin.}^{ult}\ [kN]$ |
|---|---|---|---|
| 80° | 1209 | 6857 | 6963 |
| 60° | 1634 | 2829 | 3267 |
| 50° | 1638 | 1952 | 2549 |
| 40° | 1630 | 1368 | 2128 |
| 30° | 1628 | 940 | 1879 |
| 10° | 1611 | 285 | 1636 |

Figure 9 shows the comparison of the failure envelope based on the axial, lateral and inclined loading conditions from the present model and an analytical method suggested by Supachawarote, et al. (2004). The analytical solution is the following:

$$\left(\frac{H}{H_0}\right)^a + \left(\frac{V}{V_0}\right)^b = 1 \qquad (2)$$

Where a and b constants are the following:
a = L/D+0.5 and b = L/3D+4.5.

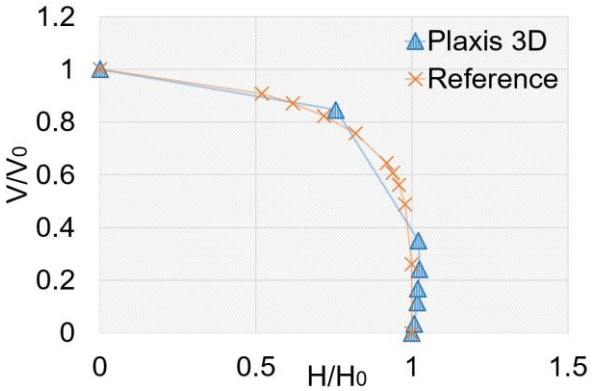


*Figure 9 V-H failure envelope for inclined loading in clay with linearly increasing shear strength*

As it seems the resulted V-H failure envelope from Plaxis 3D is in very good agreement with the reference line. A better fit could have been obtained with more loading inclinations.

## 4 CONCLUSIONS

The failure mechanisms of a suction caisson with D/L equal to 1, in dense sand and normally consolidated clay has been investigated by means of numerical modelling in this study. In the case of dense sand the increase of the dilation angle was shown to increase the axial bearing capacity. The different constitutive models employed indicate a different distribution of the deviatoric strains, hence the failure surfaces in HSsmall model are less distinct as there is less strain localization. Shaft failure occurs in case of inclined loading without clearly visible, expanded failure zone. The combined failure envelope is in good agreement with the one suggested by Byrne (2000).

The modelling of the ultimate load in case of normally consolidated clay showed a higher bearing capacity in terms of pure horizontal and vertical loading for clay with an undrained shear strength linearly increasing with depth. The obtained failure envelope was fitted with an ellipsoidal function proposed by Supachawarote et al. (2004), with a good agreement.

## 5 REFERENCES


Andersen, K. H., Murff, J. D., Randolph, M., Clukey, E. C., Erbrich, C. T., Jostad, H. P., & Supachawarote, C. (2005). Suction anchors for deepwater applications. Proceedings of the International Symposium on Frontiers in Offshore Geotechnics (ISFOG). (M. Cassidy & S. Gourvenec (eds)), CRC Press/Balkema, The Netherlands, 3-30.

Benz, T. (2006). Small-Strain Stiffness of Soils and its Numerical Consequences, Mitteilung des Instituts für Geotechnik der Universität Stuttgart. Germany. Stuttgart.

Bolton, M. D. (1986). The strength and dilatancy of sands. Geotechnique, 36(1), 65-78.

Brinkgreve, R. B. J., Kumarswamy, S. & Swolfs, W. M. (2015). Plaxis 3D Anniversary Edition Manual. Plaxis bv. The Netherlands. Delft.

Butterfield, R. & Gottardi, G. (2003). Determination of yield curves for shallow foundations by "swipe" testing. Magnan et Droniuc ed. Presses de l'ENPC/LCPC. France. Paris.

Byrne, B. W. (2000). Investigation of Suction Caissons in Dense Sand. PhD Dissrtation, Magdalen College. The United Kingdom. Oxford.

Chen, W. F. & Liu, X. L. (1990). Limit analysis in soil mechanics. Elsevier Science Publishers. Development in Geotechnical Engineering. The Netherlands. Amsterdam.

Houlsby, G. T. (1991). How the Dilatancy of Soils Affects Their Behaviour. Soil Mechanics Report (OUEL1888/91) University of Oxford, Department of Engineering Science. The United Kingdom. Oxford.

Houlsby, G. T., Ibsen, L. B. & Byrne, B. W. (2005). Suction caissons for wind turbines. Proceedings of the International Symposium on Frontiers in Offshore Geotechnics (ISFOG). (M. Cassidy & S. Gourvenec (eds)), CRC Press/Balkema, The Netherlands, 75-93.

Larsen, K. A., Ibsen, L. B. & Barari, A. (2013). Modified Expression for the Failure Criterion of Bucket Foundations Subjected to Combined Loading. Canadian Geotechnical Journal, 50(12), 1250–1259.

Lyamin, A. V., Salgado, R., Sloan, S. W. & Prezzi, M. (2007). Two- and three-dimensional bearing capacity of footings in sand. Géotechnique, 57 (8), 647-662.

Potts, D. M. & Zdravkovic, L. (1999). Finite element analysis in geotechnical engineering: theory. Thomas Thelford Publishing. The United Kingdom. London.

Senders, M. & Kay, S. (2002). Geotechnical suction pile anchor design in deep water soft clays. Proceedings of Conference Deepwater Risers Mooring and Anchorings. The United Kingdom. London.

Senders, M. (2008). Suction caissons in sand as tripod foundations for offshore wind turbines. PhD Dissertation, University of Western Australia, Perth, Australia.

Supachawarote, C., Randolph, M. & Gourvenec, S. (2004). Inclined Pull-out Capacity of Suction Caissons. Proceedings of The International Society of Offshore and Polar Engineers. France. Toulun.

Vaitkunaite, E., Molina, S. D. & Ibsen, L. B. (2012). Comparison of Calculation Models for Caisson Foundation in Sand. Department of Civil Engineering, Aalborg University, DCE Technical Memorandum; No. 17. Denmark. Aalborg.

Yun, G. & Bransby, M. F. (2007). The Undrained Vertical Bearing Capacity of Skirted Foundations. Japanese Geotechnical Society. Soils and Foundations, 47(3), 493-505.